Weather and Climate Extremes 28 (2020) 100238

Contents lists available at ScienceDirect

Weather and Climate Extremes

journal homepage: http://www.elsevier.com/locate/wace

Tracking Iberian heatwaves from a new perspective

Antonio Sánchez-Benítez [a,b,*], David Barriopedro [b], Ricardo García-Herrera [a,b]

[a] Departamento de Física de la Tierra y Astrofísica, Facultad de Ciencias Físicas, Universidad Complutense de Madrid, Madrid, Spain
[b] Instituto de Geociencias (IGEO), CSIC-UCM, Madrid, Spain

A B S T R A C T

This paper presents a new heatwave (HW) detection algorithm that identifies spatially coherent HW patterns on synoptic scales and their temporal evolution, yielding the main characteristics (extension, intensity or persistence) of HW events (HWEs). The algorithm has been applied to temperature data from the ERA-Interim reanalysis in order to derive a catalogue of Iberian HWEs for the extended summers (June to September) of the 1979–2017 period. The results indicate mean frequencies of five Iberian HWEs and 16 summer days with HW conditions over Iberia (Iberian HWDs), with significant positive trends in both diagnostics. The analysis of the life-cycle reveals that more than half of the HWEs correspond to events that originated within the region. Although Iberian HWEs last more than one week on average, they tend to be transient, persisting for about three days in the region (Iberian phase), where they reach maximum intensity and extension, and evolving later to other areas. In order to identify recurrent patterns of occurrence, a clustering of Iberian HWEs was performed based on their mean temperature fields. Four clusters were obtained: Atlantic, Subtropical, European and Mediterranean events, which display distinctive characteristics and spatio-temporal evolution, causing HW conditions in western, southern, northern and eastern Iberia, respectively. Interestingly, Mediterranean events largely explain the overall trends in Iberian HWEs and HWDs.

The connection between Iberian HWEs and atmospheric circulation patterns as summarized in four Weather Regimes (WRs) was also investigated. During the Iberian phase, HWEs are preferentially associated with ridge conditions in western Europe, with small variations in this WR determining different regional HWEs. However, the four types of regional Iberian HWEs tend to occur under different WRs during their pre- and post-Iberian phases, and show different relationships with WRs on seasonal scales. Using an impact-oriented metric for HWEs that accumulates the intensity of HW conditions over the areas affected by the event through its life-cycle, the top 10 Iberian HWEs were identified. They include well-known recent events such as those of August 2003, and June 2017. Flow analogues of the most outstanding Iberian HWEs reveal that recent warming has contributed to double their extension and intensity, making them more exceptional than they would have been in the past.

1. Introduction

Europe has warmed up in the last decades at a rate of around 0.2 °C decade^{-1} and this trend is expected to continue in the future (Hartmann et al., 2013). The recent warming is even more evident in the Mediterranean region, where climate change projections anticipate a pronounced warming and increases in inter-annual warm-season variability and droughts (Polade et al., 2017; Byers et al., 2018). Other evidence agrees that Euro-Mediterranean heatwaves (HWs from now on) are becoming more frequent, intense, and are extending to earlier dates (Barriopedro et al., 2011; Meehl and Tebaldi, 2004; Russo et al., 2015; Sánchez-Benítez et al., 2018), thus leading to an extension of the summer season (Peña-Ortiz et al., 2015). These events often cause large socio-economic impacts, which include increased mortality (Fouillet et al., 2006), extensive crop failures (Lesk et al., 2016), devastating wildfires (Hodzic et al., 2007; Gouveia et al., 2016) and poor air quality (Vautard et al., 2005; Tressol et al., 2008; Konovalov et al., 2011; Ordoñez et al., 2017). Among the most severe episodes in western Europe are the August 2003 HW event (HWE), which caused 70000 heat-related fatalities and US$10 billion of economic losses (García-Herrera et al., 2010), and the recent June 2019 HWE (Sousa et al., 2019).

Until now, HWs have been studied from an Eulerian perspective (the term Eulerian is herein used by analogy with the fluid mechanics). This approach emphasizes local aspects of HWs such as their associated impacts, but the diagnosed events are treated separately (and somehow assumed independent) from those occurring in neighbour areas (Perkins and Alexander, 2013). In particular, this description is not suitable to diagnose HWs on synoptic scales, which show changing patterns along their life-cycle, affecting widespread regions simultaneously and sometimes leading to intermittent HWs conditions in some locations. This limitation becomes particularly acute for outstanding HWs, also referred to as mega-heatwaves, characterized by extreme long-lasting conditions over widespread areas. To illustrate this, Fig. 1 shows snapshots of the 2003 HWEs, as detected by an Eulerian method that identifies local events from the exceedance of the 95th percentile of the local daily mean

* Corresponding author. Instituto de Geociencias, CSIC-UCM, Madrid, Spain.
E-mail address: antsan08@ucm.es (A. Sánchez-Benítez).

https://doi.org/10.1016/j.wace.2019.100238
Received 5 April 2019; Received in revised form 8 November 2019; Accepted 11 November 2019
Available online 14 November 2019

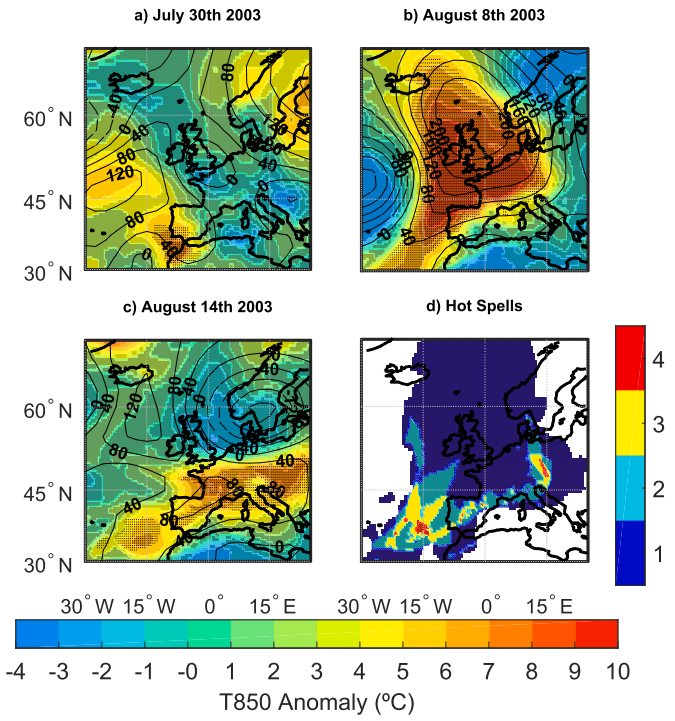

Fig. 1. a-c) Temperature (shading, in °C), and Z500 (contours, in m, with contour interval of 40 m) anomalies for snapshots of the August 2003 HWE. Grid points under local HW conditions are shown with dots; d) Number of hot spells (i.e. HW periods separated by at least one non-HW day) in each grid point for the July-August 2003 HWE.

temperature distribution at 850 hPa. HW conditions extended over large areas and persisted for long time, in agreement with the large-scale, long-lasting character of the event, but they affected different regions at different times. As such, from a local perspective, the event could have been erroneously diagnosed as different and apparently unconnected hot spells (Fig. 1). Some of these shortcomings also affect to Eulerian-based diagnostics of HWEs. For example, Russo et al. (2015) recently introduced an index that accounts for the accumulated amplitude and persistence of local HW conditions during each summer (the Heatwave Magnitude Index daily, HWMId). By construction, this index ranks summers and not individual events, and hence it does not allow quantifying the relative contribution of HWEs that occur within the same season (e.g. in addition to the August 2003 mega-heatwave, several regions were also affected by a HWE event in June 2003).

Therefore, the Eulerian description can lead to a misperception of synoptic HWs, whose surface fingerprint is largely dictated by the spatio-temporal evolution of the atmospheric circulation. This is supported by previous studies that have shown the importance of the atmospheric circulation in the occurrence of HWs. For example, Jézéquel et al. (2018a) found that it explained more than 50% of the observed temperature anomalies in three out of the four most outstanding HWs in western Europe between 2003 and 2015. Sánchez-Benítez et al. (2018) reported that the dynamics contributed to more than two thirds of the observed temperature anomalies in the June 2017 HWE. The dynamic control of synoptic HWs has motivated recent studies on the connection between Weather Regimes (WRs) and the frequency of hot extremes in Europe (Horton et al., 2015; Álvarez-Castro et al., 2018). They found more frequent summer hot extremes over Europe during WRs associated with a ridge or blocking over central Europe.

Several studies have already reported a human fingerprint in recent HWEs (e.g. Stott et al., 2003; Otto et al., 2012). However, the detection/attribution mainly concerned thermodynamic aspects of climate change, with dynamical changes remaining more controversial (Shepherd, 2016). Some recent efforts based on flow analogues (e.g. Yiou et al., 2017; Vautard et al., 2016 and references therein) have aimed to quantify dynamical changes in episodes (Sánchez-Benítez et al., 2018) or peak days (Jézéquel et al., 2018b) of recent HWs. By inferring the probability distribution expected in a given climatological period from the atmospheric circulation at the time of the event, the analogue method also yields a probabilistic attribution of the event intensity/-frequency to climate change, regardless its causes (Stott et al., 2016 and references therein). However, there are no detection/attribution exercises focusing on the characteristics of the event itself (spatial extension, persistence, etc.), which would allow a simpler interpretation of dynamical changes.

In the paper, we present a Lagrangian-inspired algorithm to identify and characterize HWs from daily gridded temperature fields. Different to the Eulerian approach, which provides a catalogue of local exceedances, the Lagrangian method analyses the whole temperature field and identifies events with a certain spatio-temporal structure. This approach also provides a list of attributes to characterize the events such as their spatial extension, persistence or intensity. The resulting catalogue emphasizes the synoptic character of HWs, filtering local HWs and hence provides an easier framework to interpret the dynamics in terms of the associated circulation. The algorithm works on global or continental scales and on different spatial resolutions, and the analysis of the so-detected events can be further confined to specific regions and seasons. Here we focus on summer (June-to-September) HWs over Iberia and yield a climatological analysis using reanalysis data. This choice is motivated by the following reasons: i) Iberia is placed on the Mediterranean region, which has been identified as a climate change hot spot, with pronounced projected increases in HWs (Perkins, 2015; Lelieveld et al., 2016; García-Herrera and Barriopedro, 2018; Hoegh-Guldberg et al., 2018); ii) To the best of our knowledge, studies on this region have mostly focused on trends in observed or simulated extreme temperature indices at local scales following an Eulerian-based approach (Rodríguez-Puebla et al., 2010; Ramos et al., 2011; Fernández-Montes and Rodrigo, 2012, 2015; Acero et al., 2014; Morabito et al., 2017; Tomczyk et al., 2017) instead of addressing the characteristics of synoptic HWEs. Although these works report an increasing frequency or intensity of extreme indices over Iberia in the last decades, it is unclear how these trends impact on the morphology of Iberian HWEs; iii) From a climatological point of view, Iberia is located in a transition area and is frequently affected by HW-related weather systems that are typical of both subtropical and extratropical regions (e.g. Sousa et al., 2018).

This paper is structured as follows. In the next section, the data and methods used for the analysis of HWs are presented, with special emphasis on the description of the detection algorithm. The main results are described in section 3, including the climatology of Iberian HWs, their association with Euro-Atlantic WRs, the identification of regional HW patterns and trends, and a more detailed assessment of the top ten Iberian HWs. Finally, section 4 summarizes the main conclusions.

2. Data and methods

2.1. Data

Daily mean fields, including geopotential height at 500 hPa (Z500), temperature at 2 m (T2m) and 850 hPa (T850), were obtained from the ERA-Interim reanalysis (Dee et al., 2011) with a 0.5 × 0.5° resolution for the 1979–2017 period for the extended summer (June-September). For comparative purposes, the same fields were also extracted on a lower resolution grid (2.5° x 2.5°) both from the ERA-Interim reanalysis in the 1979–2017 period and from the National Centres for Environmental Prediction/National Center for Atmospheric Research (NCEP/NCAR) reanalysis (Kalnay et al., 1996) for a longer period (1948–2017). Through this paper, daily anomalies were computed by removing the 1981–2010 mean for each calendar day.

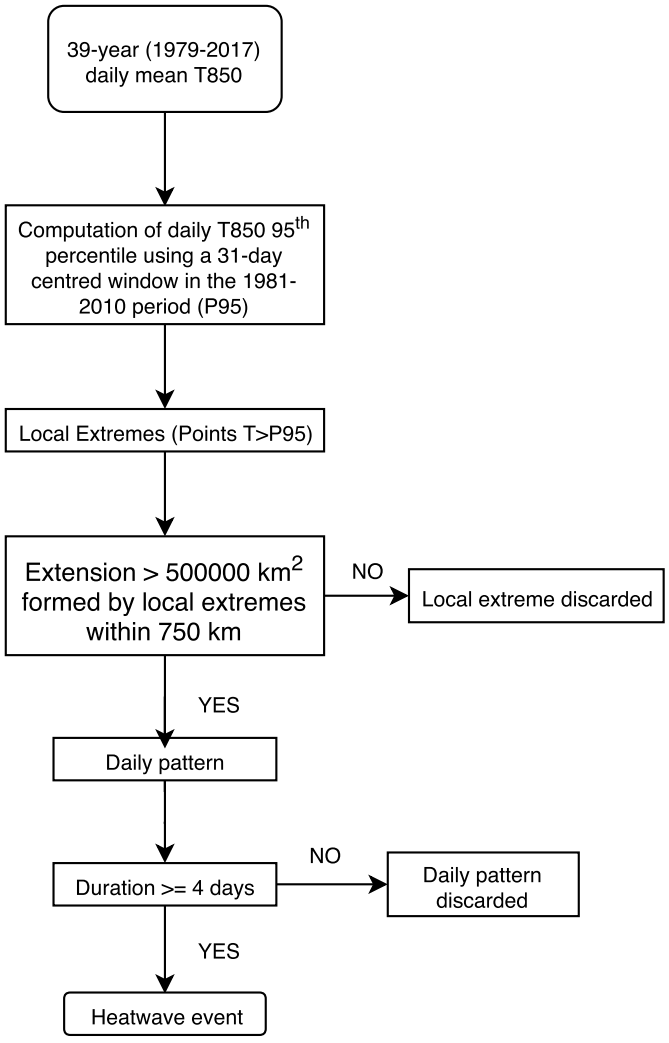

Fig. 2. Schematic of the HW detection algorithm.

2.2. A novel detection algorithm

Herein, we propose a change in the perspective of HWs analysis. We have designed a novel algorithm that focuses on the spatial pattern of extreme temperatures and its evolution. It works as follows (Fig. 2): For each day we identified grid points (oceanic regions included) exceeding a local temperature threshold, referred to as local extremes. This threshold is defined for each grid point and calendar day as the 95th percentile of the daily T850 distribution constructed from all 31-day intervals of the 1981–2010 period centred on that day. The width of these intervals was chosen as a compromise to obtain a smoothed evolution of that threshold but without underestimating the amplitude of its seasonal cycle. T850 is better suited than T2m to detect synoptic scale HWs, because it is smoother and less affected by surface effects such as orography. Then, we searched for areas with a high concentration of local extremes (hereafter referred to as daily patterns). They are formed by local extremes separated by less than 750 km covering a total area of at least 500,000 km^2. The first distance threshold is close to the Rossby radius of deformation at midlatitudes (Lr), and was used to merge clusters of local extremes that are unconnected but sufficiently close to be affected by the same weather system. The extension threshold ($\sim Lr^2$) allows filtering small scale and isolated extremes, without restricting the detection to mega-heatwaves. Daily patterns are characterized by several parameters derived from their embedded local extremes: the areal extension (in km^2), the intensity (in standard deviations, measured by the area-weighted mean standardized temperature anomaly) and the centre location (the mean longitude and latitude weighted by the temperature anomaly).

The second part of the algorithm tracks the evolution of daily patterns in order to identify HWEs (Fig. 2). A pattern of day d+1 is considered the continuation of another one detected on day d if one of these two conditions is satisfied: 1) their areas overlap by at least 50% (quasi-stationarity); 2) there is some overlap between the patterns and the distance between their centres is lower than 1 000 km. The latter condition was required to allow for eventual abrupt changes in the spatial pattern and/or the areal extension. If a daily pattern is tracked for at least four days it is considered a HWE. All days belonging to a given HWE are referred to as HW days (HWDs from now on).

These criteria and the chosen thresholds were tested during well-known European events. The results reported herein still hold for small changes in these thresholds. To further evaluate the algorithm on subcontinental scales, we selected HWEs that affected any grid point of Spain for at least one day during their life-cycle. They were compared with an independent list of Spanish HWEs (AEMET, 2018) based on land observations from weather stations. HWEs are therein defined as exceedances of the local 95th percentile of daily maximum T2m for July-August days of the 1971–2000 period occurring in at least 10% of the stations during three or more consecutive days. We stress that stations are not homogeneously distributed and the extension threshold can be satisfied by a cluster of nearby stations extending over $\sim 10^4$ km^2 (i.e. one order of magnitude lower than our extension criterion) or by sparse stations that are far away. In spite of the differences in the underlying data and the methodology (observations vs. reanalysis, Eulerian vs Lagrangian, local stations vs. grid points, daily maximum T2m vs. daily mean T850), a cross-comparison using thresholds in our algorithm similar to those employed by AEMET yielded a similar frequency of HWEs, capturing more than 75% of the AEMET HWEs in the 1979–2016 period. Missed HWEs of the AEMET list often affected localized areas of Spain, thus being filtered out by the algorithm. In addition, the algorithm has already proven its ability to identify and track European mega-heatwave events, such as the June 2017 HWE (Sánchez-Benítez et al., 2018) or the June 2019 HWE (Sousa et al., 2019). Finally, the results described in this paper with the ERA-Interim reanalysis at 0.5° x 0.5° spatial resolution are also similar to those obtained from the same reanalysis at a lower spatial resolution (2.5° x 2.5°) and from the NCEP/NCAR reanalysis, despite the lower frequencies of HWEs in the latter cases. Therefore, the algorithm's performance is not very sensitive to the reanalysis and grid used.

From the continental catalogue we selected the subset of HWEs that affected any grid point of Iberia for at least one day (referred to as Iberian HWEs). Note that Iberian HWEs do not necessarily affect this region during their whole life-cycle. Therefore, some of the subsequent analyses were restricted to those HWDs of each Iberian HWE with HW conditions on at least one land grid point of Iberia (Iberian HWDs hereafter). To evaluate long-term changes in HWEs and HWDs, their trends were computed as the slope of the linear regression. Their statistical significance was assessed with the ρ-Spearman test, which is more robust than parametric tests and less affected by the presence of outliers (Lanzante, 1996).

Iberian HWEs were ranked according to an adapted version of the HWMId index of Russo et al. (2015) that integrates the intensity, spatial extension and persistence of HWEs into a single index, herein referred to as Heatwave Magnitude Index event (HWMIe), which yields one value per HWE. The HWMId index normalizes the temperature anomaly using the interquartile range as follows (Russo et al., 2015):

$$HWMId_{i,j} = \begin{cases} \dfrac{T_d - T_{25p}}{T_{75p} - T_{25p}} & if\ T_d - T_{25p} > 0 \\ 0 & if T_d - T_{25p} \leq 0 \end{cases}$$

where T_d is the local daily mean T850 of day d and T_{25p} (T_{75p}) is the corresponding 25th (75th) percentile of that calendar day computed

from all 31-day centred windows of the 1981–2010 period. For a given HWE, the area-weighted HWMId mean for the grid points of each instantaneous pattern (HWMI hereafter) is first computed and these daily values are later accumulated over the life-cycle of the HWE to yield HWMIe:

$$HWMI = \sum_{i,j} HWMId_{i,j} * \cos(lat_j)$$

$$HWMIe = \sum_{d} HWMI$$

where i and j are the longitude and latitude, and d is each day of the HWE. As the HWMIe aims to quantify the integrated effects of Iberian HWEs from an impact-oriented perspective, the sum is only accumulated over inland HW grid points of Iberia. This approach allows us to provide a metric for HWEs by taking into account the persistence, spatial extent and intensity of HW conditions over the land area affected by their spatial patterns.

2.3. Weather regimes and regionalization of heatwaves

The Self Organized Maps technique (SOM, Kohonen, 2001; Crane and Hewitson, 2003) was used to identify WRs over the European sector (Horton et al., 2015). SOM uses a neural network and an unsupervised and iterative learning process to identify recurrent spatial patterns by grouping days with similar 2D data distribution. Unlike other clustering algorithms, SOM avoids assumptions on data distribution and is trained during the data processing (Cassano et al., 2006). To identify WRs, we used the standardized Z500 anomaly field over the region [30-60°N, 35°W-35°E] for all June-September days, retaining four WRs, as in Horton et al. (2015). The daily catalogue of WRs allows classifying Iberian HWDs into one of the four WRs.

The SOM was also applied to T850 fields in order to identify recurrent temperature patterns associated with Iberian HWEs. To do so, we first computed the mean spatial pattern of standardized T850 anomaly for all Iberian HWDs of each HWE, thus obtaining one pattern per Iberian HWE. SOM was then applied to classify Iberian HWEs according to their mean T850 patterns over the region [30–70 °N, 35°W-35°E]. This yields a regionalization of Iberian HWEs, whose parameters can be compared. A Monte Carlo test of 100,000 iterations was used to assess the significance of the HWE parameters of each cluster. In each iteration we randomly selected the same number of HWEs as cases are included in the given cluster and computed the mean HWE parameters. For each parameter, this provides a random distribution, against which the mean HWE parameter of the cluster is compared. The latter is significant at the 95 (99) % confidence level if it lies above the 97.5th (99.5th) or below the 2.5th (0.5th) percentile of the random distribution.

2.4. Detection of changes in heatwaves

Recent studies have applied the analogue method to quantify the dynamical contribution to near-surface anomalies during extreme events and in detection and attribution of extreme events to climate change (e.g. Stott et al., 2016; Yiou et al., 2017). The latter requires searching for flow analogues of the extreme event in two different climatological periods. Herein, we searched for flow analogues of the ERA-Interim Iberian HWEs in past (1948–1978) and present (1979–2017) subperiods. To do so, the NCEP/NCAR reanalysis was used as it covers a longer period than ERA-Interim. The analogue technique employed in this work follows Jézéquel et al. (2018a). Accordingly, for the Z500 NCEP/NCAR field of each Iberian HWD, we looked for the N = 20 days of each subperiod with the nearest Z500 anomaly fields. The search was restricted to the (−30, +30) interval of the corresponding calendar day, and the distance criterion is defined by the Euclidean distance over the [30-70°N, 35°W-35°E] region. Different choices in the spatial domain or the number of circulation analogues were tested, yielding similar results. For each of the N analogues, we first verified if an Iberian HWE was detected, and if so, retained the instantaneous pattern and the corresponding parameters. Then, we randomly picked one of the N analogues and repeated this process for each day of the considered Iberian HWE, thus reconstructing the mean 2-D field and parameters for its life-cycle. This process was repeated 100,000 times in order to derive a statistical distribution. This method tends to underestimate the parameters of these events, as it only takes into account the dynamics. The remaining could partially be explained by other amplifying factors not accounted for by the circulation (e.g., land-atmosphere feedbacks or SST anomalies). Note that these limitations apply to both subperiods and hence do not prevent their comparison. The resulting differences in HW characteristics should be attributed to changes in the climatology and allow us to infer how these HW events could have been in the past period. The significance of the differences was computed using a Mann-Withney U test.

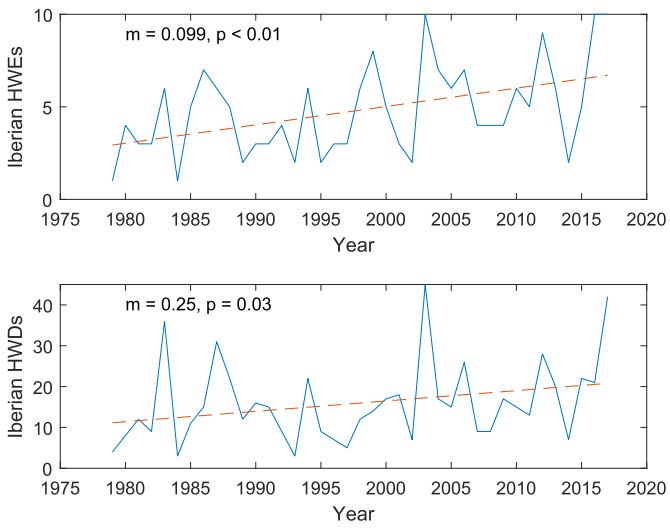

Fig. 3. Extended summer frequency of (top) Iberian HWEs (in number of events) and (bottom) Iberian HWDs (in days) for the 1979–2017 period. The dashed line indicates the adjusted linear trend.

3. Results

3.1. Climatology of Iberian heatwaves

A total of 188 Iberian HWEs were detected in the 1979–2017 period, leading to 623 Iberian HWDs. There were no days with more than one HWE over Iberia and hence HWEs affected Iberia for 3.3 days, on average. The time series of Iberian HWEs and HWDs are shown in Fig. 3. Iberian HWEs occurred in all years of the analysed period, with a maximum of 10 in 2003 and 2017. The 2003 summer also displayed the highest number of Iberian HWDs (a total of 45). Further analyses indicate a relatively small intraseasonal variability of Iberian HWEs, with slightly higher frequencies in August and lower cases in September (not shown). The occurrence of Iberian HWEs and HWDs has increased in the 1979–2017 period, with significant positive trends of +1.0 HWE decade^{-1} and +2.6 HWDs decade^{-1}, respectively. The resulting catalogue is similar to those obtained with NCEP/NCAR and ERA-Interim at 2.5°x2.5° resolution. In these cases, the frequency of Iberian HWEs and HWDs is reduced by ~20–30% and 15–25% respectively, but trends are still significant at $p < 0.01$ and $p < 0.1$ level (Fig. S1).

Iberian HWEs affect Iberia for 3.3 days on average, the trend in HWEs should translate into a trend of +3.3 HWDs decade^{-1}. As the actual trend of HWDs is lower than that, we infer that Iberian HWEs have become more transient. This hypothesis is confirmed by computing the trend in HWEs persistence over Iberia, which shows decreasing

Table 1
Characteristics (mean and standard deviation) of Iberian HWEs (last column) and regional Iberian HWEs (columns two to five) for 1979–2017. * (**) Symbol indicates significant trends at $p < 0.05$ (0.01) level.

Iberian HWEs characteristics	Atlantic	Subtropical	European	Mediterranean	All
Pre-Iberian phase (days)	1.8 ± 2.6	1.9 ± 3.3	1.3 ± 2.6	1.8 ± 4.1	1.7 ± 3.2
Iberian phase (days)	3.5 ± 3.0	3.7 ± 3.5	3.5 ± 2.5	2.6 ± 2.1	3.3 ± 2.8
Post-Iberian phase (days)	2.5 ± 2.4	3.9 ± 3.4	2.4 ± 2.9	5.0 ± 5.9	3.4 ± 3.9
Mean extension pre-Iberian phase (10^6 km^2)	2.1 ± 2.2	2.3 ± 1.5	1.8 ± 1.1	2.0 ± 1.5	2.1 ± 1.7
Mean extension Iberian phase (10^6 km^2)	2.7 ± 2.7	3.6 ± 3.7	2.2 ± 1.4	2.2 ± 1.7	2.6 ± 2.5
Mean extension post-Iberian phase (10^6 km^2)	1.7 ± 0.8	2.8 ± 1.8	1.5 ± 0.7	1.8 ± 1.0	1.9 ± 1.2
Affected Iberian area (10^5 km^2)	1.4 ± 1.1	1.5 ± 1.1	1.6 ± 1.6	0.8 ± 0.9	1.3 ± 1.2
Iberian HWEs trend (HWEs decade^{-1})	0.19	0.15	0.08	0.57**	0.99**
Iberian HWDs trend (HWDs decade^{-1})	0.08	0.39	0.64	1.44**	2.54*
HWMIe (10^2)	4.1 ± 6.1	4.3 ± 6.2	4.6 ± 6.2	1.7 ± 3.0	3.6 ± 5.6

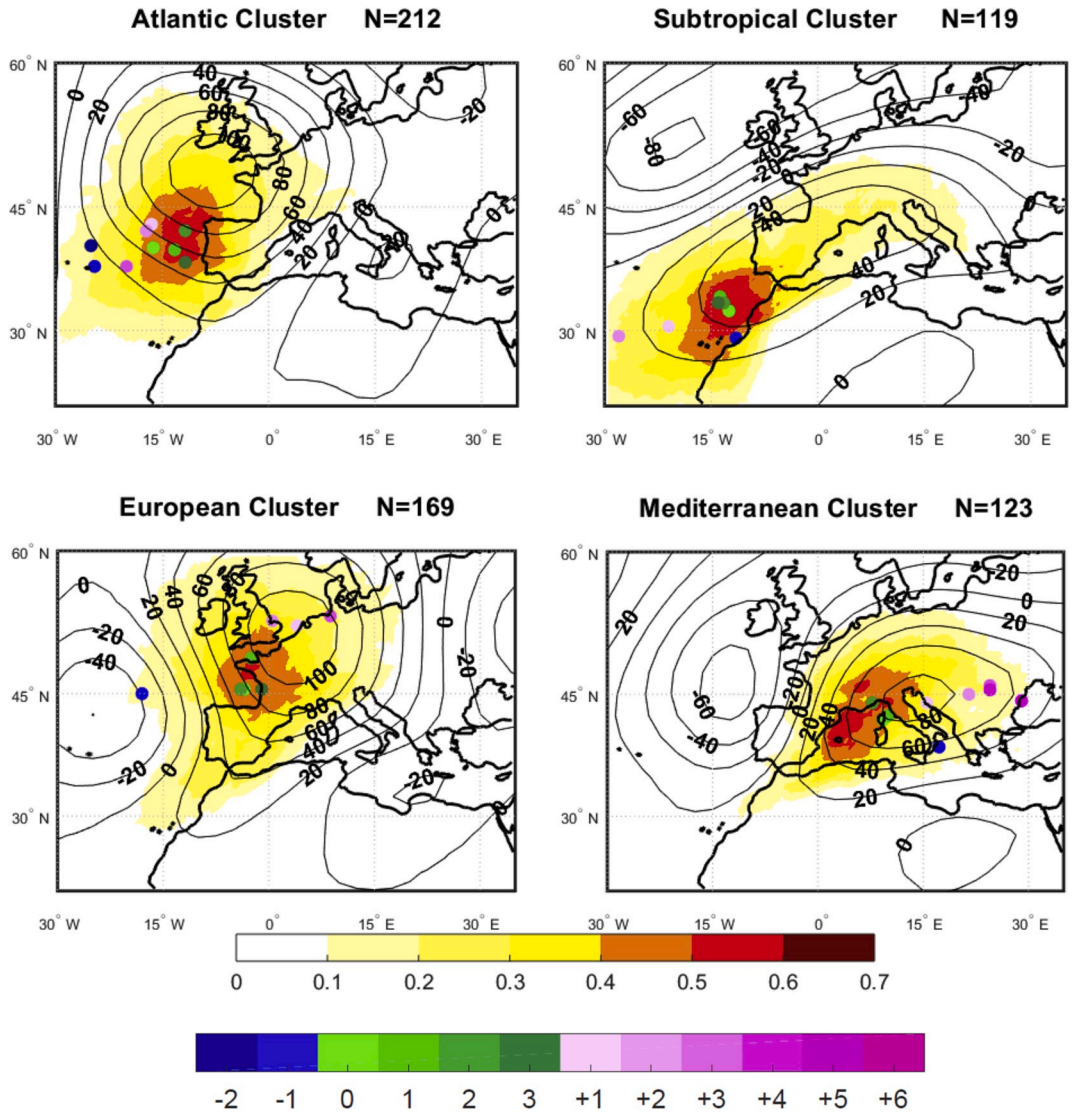

Fig. 4. Composite of HWD frequency (shading, in percentage with respect to the total number of days in the cluster, top colourbar), Z500 anomaly (contours, in m) and centre location (dots, bottom colourbar) for the 1979–2017 Iberian HWEs of each cluster. The number of days included in each cluster is indicated.

values. It is not statistically significant at $p < 0.05$, though (not shown), being overwhelmed by the positive trend in the frequency of HWEs. Therefore, the upward trend of HWDs is due to the increase of HWEs. The remaining parameters (i.e. extension and intensity) do not show significant trends at $p < 0.05$.

As our algorithm focuses on synoptic HWEs patterns instead of local events, it can also draw information on their spatio-temporal evolution, including periods before (pre-Iberian phase), during (Iberian phase) and after (post-Iberian phase) they affect Iberia. A summary of the main characteristics of Iberian HWEs is provided in Table 1 (last column). These parameters display large standard deviation values (even higher than the mean in some of them), pointing to substantial variability among events. This is typical of extreme events, and was expected from the large spectrum of targeted scales, as well as the transient behaviour

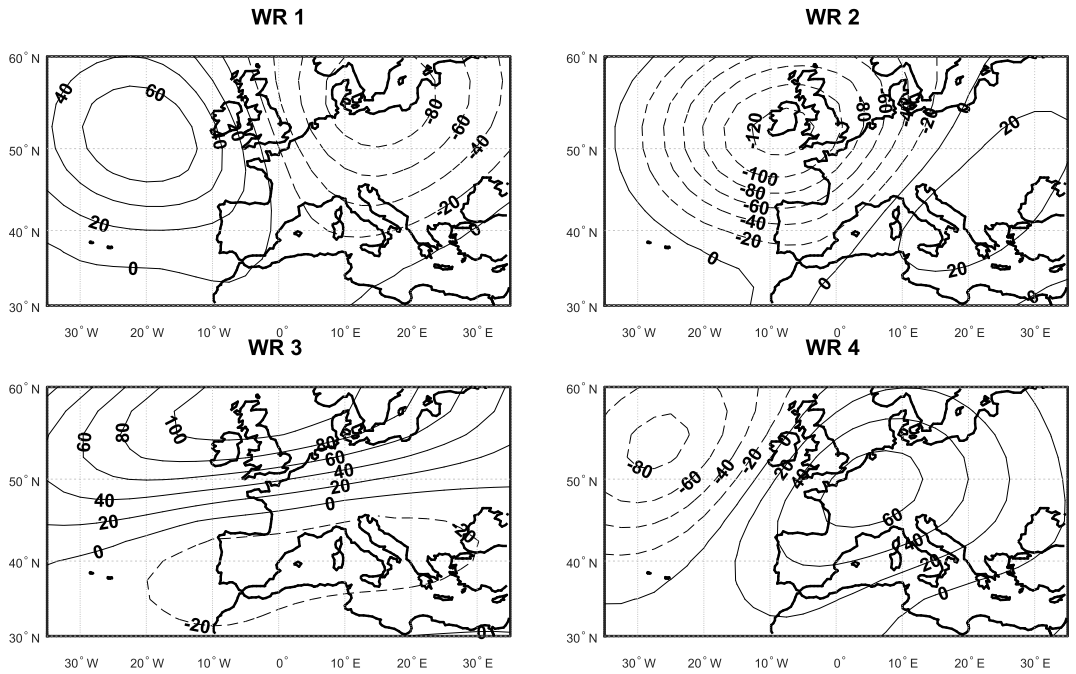

Fig. 5. Composites of Z500 anomalies (contours, in m) for the extended summer days of 1979–2017 classified in each WR.

and diversity of weather systems associated with HWs in the region, which translates to high standard deviations in HWE parameters. HWEs persistence in the pre-Iberian phase was considerably lower than in the post-Iberian phase (1.7 vs 3.4 days/event). Indeed, more than half HWEs (55.4%) already hit this region the first day they were detected, indicating that Iberia is a favourable region for the build-up of synoptic HW conditions. The areal extent of HWEs tends to peak in the Iberian phase, when it reaches a mean extension of 2.6 million km^2. Note that most of the areal extension covered by HWEs during this phase lies over the ocean. Actually, the Iberian area affected by these events is on average one order of magnitude lower (around 20% of Iberia), meaning that Iberian HWEs have strong regional signatures. Therefore, in the next section we derive a regionalization attending to the affected areas and search for differences among their HW characteristics.

3.2. Regional patterns

When the spatio-temporal evolution of all HWEs is considered, preferred tracks of their centres do not clearly emerge (not shown). This diversity agrees with the large variability of HWEs parameters (Table 1) and is also observed in the temperature signatures over Iberia, indicating large variability in the spatial fingerprints of Iberian HWEs. In order to identify regional differences, a SOM-based classification was performed for 1979–2017 period based on their mean T850 anomaly patterns over Iberia (see Section 2.3). As Iberian HWEs tend to cause HW conditions over 20% of the territory on average, only four clusters were retained. Fig. 4 shows the composites of relative frequency (expressed in percentage of days with respect to the number of HWDs included in the cluster) and Z500 anomalies for the HWDs of each group. Local HW frequencies are considerably higher for the Iberian phase (~60%, Fig. 4) than for the remaining stages of the life-cycle (~30%, not shown), indicating more diffuse patterns during the pre- and post-Iberian phases. These clusters are robust to changes in the resolution or the reanalysis employed (not shown). The main HW characteristics of each cluster are summarized in Table 1 (columns 2 to 5).

The first cluster (60 events) affects western Iberia, with the maximum frequency located in the eastern Atlantic (Atlantic events, hereafter), in good agreement with the positive Z500 anomaly. HWEs of this cluster have characteristics close to the average. They tend to form in the eastern Atlantic at least one day before affecting Iberia (more than 50% of them existed in the pre-Iberian phase) and move northeastward. In the post-Iberian phase, they weaken and decrease in extension (at the largest rate of all clusters) without a preferred trajectory.

HWEs of the second cluster (32 events) have their largest impact over southern Iberia and the HW frequency maximum is located over Morocco (Subtropical events, hereafter). The Z500 anomaly centre is shifted eastward of the HW maximum and located over the western Mediterranean, suggesting the advection of warm subtropical air masses. They reach the highest extension of all groups (significant at $p < 0.05$), although the affected area of Iberia is not the highest one. In most cases, they originate at least one day before affecting Iberia, when they are located in northern Africa or the subtropical Atlantic. In the post-Iberian phase, they can persist for long time (even a week) while keeping their large extension ($p < 0.01$) and moving towards southwest or northeast at a high speed.

The third group (48 events) has the HW and Z500 anomaly patterns centred over western Europe (European events, hereafter). The area of Iberia affected by these HWEs is the largest of all groups ($p < 0.05$), hitting the northern side of the Peninsula. In spite of this, they tend to be short-lived, with more than 50% of them affecting Iberia the first day of detection and decaying rapidly afterwards. During the post-Iberian phase, they move fast towards the northeast, with the lowest extension of all clusters ($p < 0.05$).

HWEs of the fourth cluster (48 events) are the most transient ones over Iberia ($p < 0.05$), where they persist for only 2.6 days on average, mainly affecting its eastern side (Mediterranean events, hereafter). This group is dominated by a Z500 anomaly dipole favouring warm advection over eastern Iberia from inland. This is the cluster with the lowest number of events already existing in the pre-Iberian phase (33.3%). In this phase, HW conditions are confined to eastern Europe and western Mediterranean (not shown). Although these events display the lowest extension over Iberia and HWMIe of all clusters ($p < 0.01$), they tend to persist many days in the post-Iberian phase (5.0 days on average, $p < 0.01$), while they evolve eastwards.

Interestingly, and despite being the shortest and smallest Iberian HWEs, the Mediterranean cluster is the only group with significant trends in HWEs and HWDs ($p < 0.01$, Table 1), explaining more than half of the total Iberian trends (57% for both variables). In fact, the

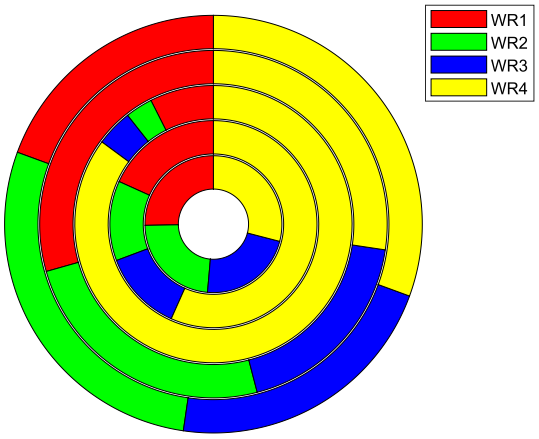

Fig. 6. WRs frequency (in percentage) for (from inside to outside): all summer days; all Iberian HWDs; HWDs of the top 10 Iberian HWEs; HWDs of the pre-Iberian phase; HWDs of the post-Iberian phase. Colours identify the WR. (For interpretation of the references to colour in this figure legend, the reader is referred to the Web version of this article.)

Iberian trends are no longer significant when Mediterranean events are removed from the pool of Iberian HWEs.

3.3. Associated atmospheric circulation

To explore the circulation patterns associated with the occurrence of synoptic Iberian HWEs, we employed the catalogue of WRs (Section 2.3) that classifies each day of the 1979–2017 period into one of the four recurrent WRs (Fig. 5). The first two WRs display a zonal dipole, with positive (negative) Z500 anomalies in the eastern Atlantic (northern-central Europe) and southeastern Europe (eastern Atlantic), respectively. WR3 depicts a meridional dipole dominated by positive Z500 anomalies near UK, that are characteristic of European blocking, and slightly negative Z500 anomalies over the Mediterranean. Finally, WR4 shows positive Z500 anomalies in western Europe, resembling the occurrence of Euro-Atlantic subtropical ridges.

From a climatological viewpoint, all WRs occur with similar frequencies (around 25%, Fig. 6, inner ring). However, when considering only Iberian HWDs there is a clear predominance of WR4. More specifically, 57% of the Iberian HWDs occurred under this WR (Fig. 6, second ring). The other WRs experience a clear reduction during Iberian HWDs, as compared with their climatological frequencies. Interestingly, the frequency of occurrence of WR4 is considerably reduced for days belonging to the pre- and post-Iberian phases of the HWEs (fourth and outer ring).

This analysis was also applied to the Iberian HWDs of each cluster of Section 3.2, separately (Fig. 7). For all clusters, the results are similar to those obtained when Iberian HWEs are considered all together: the four types of regional events are preferentially associated with WR4 during the Iberian phase. This is because during this stage all events tend to concentrate over a relatively small region (Iberia) so that their associated circulation anomalies are indistinguishable from the larger scale perspective of the WRs. Nevertheless, when we considered the pre- and post- Iberian phases we found differences among the preferred WRs of

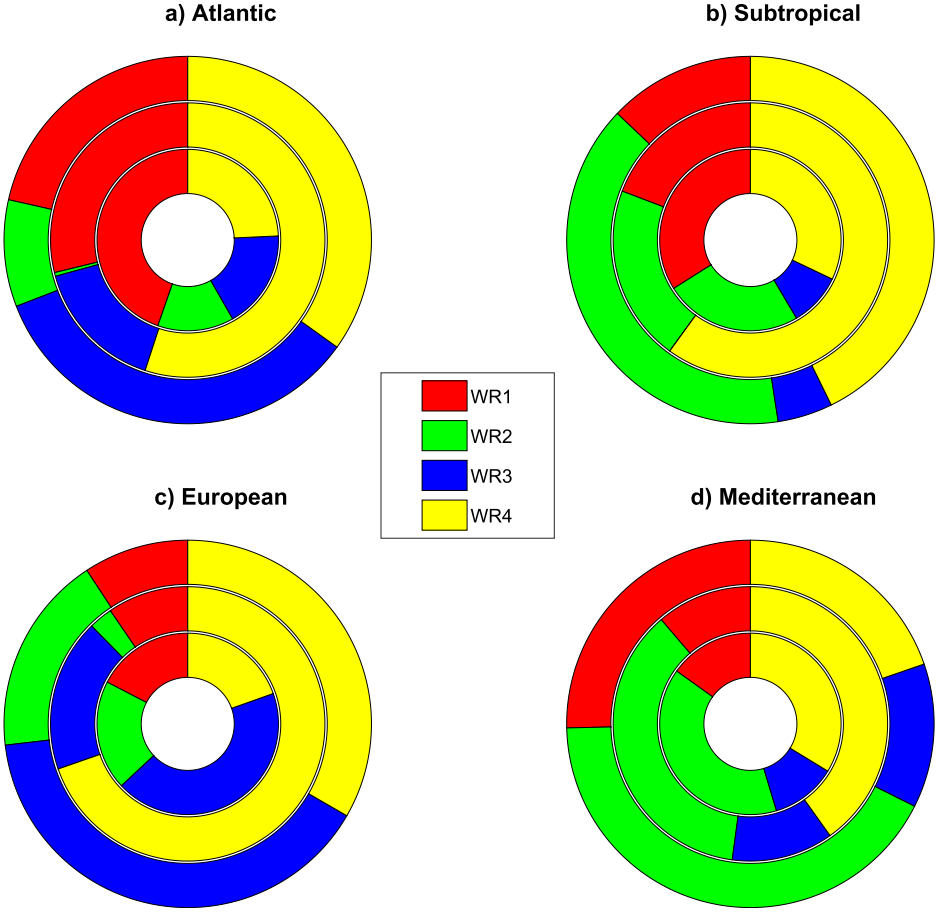

Fig. 7. WRs frequencies (in percentage) for: a) Atlantic; b) Subtropical; c) European; d) Mediterranean HWEs in the pre-Iberian (inside), Iberian (middle) and post-Iberian (outside) phases. Colours identify the WR. (For interpretation of the references to colour in this figure legend, the reader is referred to the Web version of this article.)

Table 2
Stepwise Regression model (1979–2017) for the extended summer HWD frequency of each type of Iberian regional HWE using the seasonal frequencies of WRs as predictors. Only the types for which a significant regression model is found are displayed. For each type of HWE, columns show the selected predictors, their regression coefficients (with p-values based on a *t*-test of null coefficients), the coefficient of determination (R^2) of the final regression model (with the p value of the correlation coefficient between the observed and predicted values) and the F-test statistic (with its p-value).

Type of regional Iberian HWE	WR	Coefficient (p-value)	R^2 (p-value)	F-test (p-value)
Atlantic	WR4	0.15 ± 0.05 (<0.01)	0.23 (<0.01)	4.64 (<0.05)
	WR2	−0.13 ± 0.06 (<0.05)		
European	WR4	0.16 ± 0.04 (<0.01)	0.25 (<0.01)	14.00 (<0.01)
Mediterranean	WR1	−0.19 ± 0.05 (<0.01)	0.30 (<0.01)	9.04 (<0.01)
	WR3	−0.10 ± 0.04 (<0.05)		

each cluster: WR1 is the dominant precursor of Atlantic events; Subtropical events are preferentially preceded by either WR1 or WR4; WR3 shows a clear predominance during the pre-Iberian phase of European events; Mediterranean events tend to be preceded by WR2. These results indicate that different WRs or combinations of WRs are involved through the life-cycle of regional Iberian HWEs. This stresses the importance of the assessing simultaneously the occurrence of all WRs during a given time interval.

To delve further into this issue, we explored whether WRs have some skill to anticipate the frequency of regional Iberian HWEs on seasonal scales. To do so, we applied a stepwise regression model (Wilks, 2011) for each type of Iberian HWE over 1979–2017, using the corresponding seasonal frequency of Iberian HWDs as a predictand and the extended summer frequencies of the four WRs as predictors. The stepwise regression proceeds forwards and backwards (adding and removing predictors), retaining only those predictors (if any) that improve significantly ($p < 0.05$) the explained variance of the predictand. The method identifies significant predictors for all types of regional HWEs (Table 2), with the exception of Subtropical events (which are therefore omitted in Table 2). Therefore, from a seasonal WR perspective, the predictability of Iberian HWEs varies with the type of regional event. Overall, an enhanced frequency of WR4 favours Atlantic and European events, while Mediterranean HWEs tend to be more frequent during extended summers with reduced frequencies of WR1 and WR3.

3.4. Top 10 HWEs in Iberia

As explained above, the HWMIe accounts for the intensity, persistence and affected areal extension of HWEs allowing us to rank them consistently. Here, we use the HWMIe to identify the top ten Iberian HWEs of the analysed period (1979–2017). Their main characteristics are shown in Table 3. Fig. 8 shows their spatial signatures in terms of total HWD frequency. As compared to the bulk of HWEs, these top events were associated with enhanced anticyclonic conditions, since the frequency of WR4 during these events increases from 57% to 85% (Fig. 6, third ring). Another distinctive feature of these events is their persistence over Iberia (rather than their total duration), which exceeded one week in most of the cases, thus doubling the mean duration of all Iberian HWEs.

With the exception of the September 1983, which occurred in the late extended summer, the listed events correspond to well-known episodes, supporting the performance of our algorithm and the HWMIe. The Iberian HWE of highest impact in the reanalysis period was the August 2003 event, which has been widely described in the literature (e.g. García-Herrera et al., 2010). Although the event experienced changes in extension and location (see Fig. 1), it affected most of Iberia (with the exception of the southeastern part, Fig. 8a) in all days of its life-cycle (16 days). Other well-known events are also included in the list, such as that of June 2017 (the third strongest Iberian HWE, Fig. 8c), which has recently been identified as the earliest European mega-heatwave in the reanalysis period (Sánchez-Benítez et al., 2018), or the September 2016 (8th strongest, Fig. 8h) Iberian HWEs, which caused widespread impacts over most of the territory (Zschenderlein et al., 2018).

Half of these highest-impact Iberian HWEs are European events, followed by Atlantic events (30%). Interestingly, Subtropical and Mediterranean events are underrepresented in the top ten list, as compared with their climatological frequencies. The impact of the only Mediterranean event in Table 3 (August 2012, Fig. 8j) was confined to northeastern Iberia, but it entered in the list due to its outstanding intensity (locally more than 40 °C) and persistence (eight days over Iberia), thus appearing in the 10th position. The only Subtropical event of Table 3 (September 1987, Fig. 8b) also deviated from the typical behaviour of

Table 3
Main characteristics of the top 10 Iberian HWEs of 1979–2017 ranked by their HWMIe value. Columns indicate (from left to right) the start dates, total duration (in days), mean latitude (°N) and longitude (°E), both averaged for the total duration, Iberian phase (in days), HWMIe, mean temperature anomaly averaged for each daily pattern and the type of regional Iberian HWE.

Start Date	Duration (days)	Mean Longitude (°E)	Mean Latitude (°N)	Iberian phase (days)	HWMIe (10^3)	Temperature Anomaly (°C)	Type of regional Iberian HWE
30/7/2003	16	353.8	43.0	16	3.22	5.99	Atlantic
6/9/1987	19	356.9	39.9	18	3.05	4.40	Subtropical
11/6/2017	13	357.2	43.3	13	2.90	6.72	European
5/9/1988	11	343.2	36.6	6	2.14	4.89	Atlantic
4/6/1981	23	329.5	37.0	9	1.94	4.71	Atlantic
23/9/1983	7	353.6	43.3	6	1.83	5.83	European
19/7/1995	9	355.1	43.7	7	1.71	4.83	European
4/9/2016	5	356.3	46.6	4	1.66	6.21	European
20/6/2001	7	356.1	41.6	7	1.62	4.82	European
17/8/2012	13	18.7	43.2	8	1.62	4.61	Mediterranean

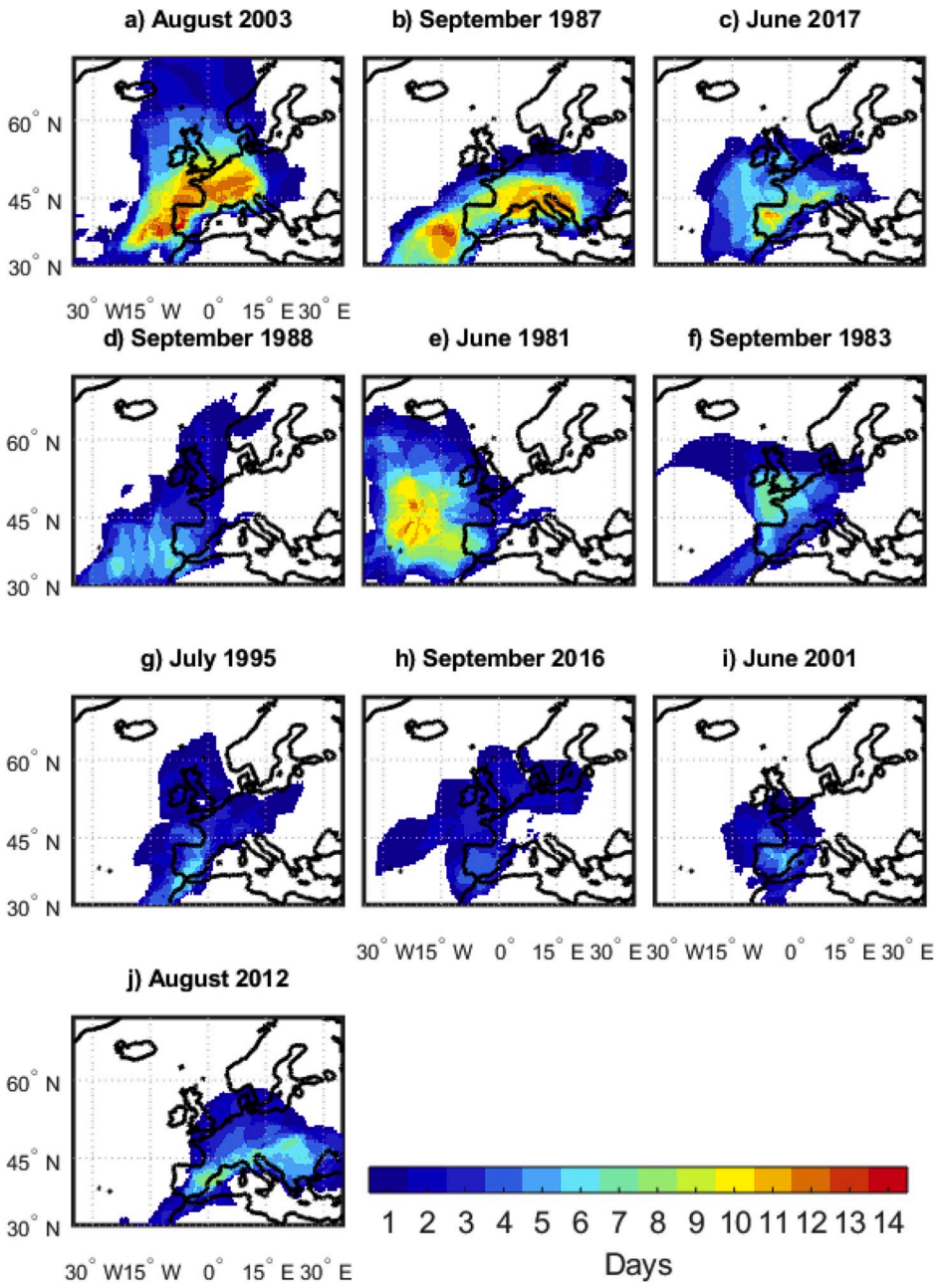

Fig. 8. Local HWD frequency (in number of days) for the top 10 Iberian heatwaves.

these events, being the most persistent in Iberia (18 days over Iberia), and causing local maxima of 12 Iberian HWDs. These aspects (long persistence and large extension) contributed to rank this event in the 2nd place.

Half of the top HWEs have occurred in the 21st century, although the 1980s was also an active decade. Taking advantage of our Lagrangian approach, we can further address how HWEs could have been in a colder climate. To illustrate this, the top three Iberian HWEs were selected, as they caused considerably widespread impacts, with HWMIe values being at least 25% larger than for the remaining top events. To do so, we have applied the analogue method in two subperiods: 1979–2017 (present) and 1948–1978 (past). This technique is justified by the large dynamical control on Iberian HWEs (Section 3.2). Indeed, preliminary analyses confirmed that the synoptic circulation explains more than 60% of the T2m anomaly associated with these Iberian HWEs, as inferred from present-day analogues (not shown). Fig. 9 shows the observed characteristics of these HWEs (extension, the affected Iberian area, number of days over Iberia and HWMIe), as well as the reconstructed values by the analogue method in both subperiods. The HWE patterns (not shown) and characteristics are reasonably reproduced by flow analogues of the present period (Fig. 9, red boxplots), taking into account the aforementioned fraction of T2m anomaly explained by the atmospheric circulation. More interesting, the three events experience significant increases (at $p < 0.01$ level) in their present-day parameters as compared to the recent past (Fig. 9, blue boxplots), indicating that these HWEs would have been less intense and persistent just a few decades ago. Specifically, climate change (herein referred to the climatological differences between the present and past subperiods) has doubled the areal extent of the most outstanding HWEs (Fig. 9a), their intensity (HWMIe, Fig. 9d) and the extension of the affected Iberian regions (Fig. 9b), also increasing by more than 50% their persistence over Iberia (Fig. 9c).

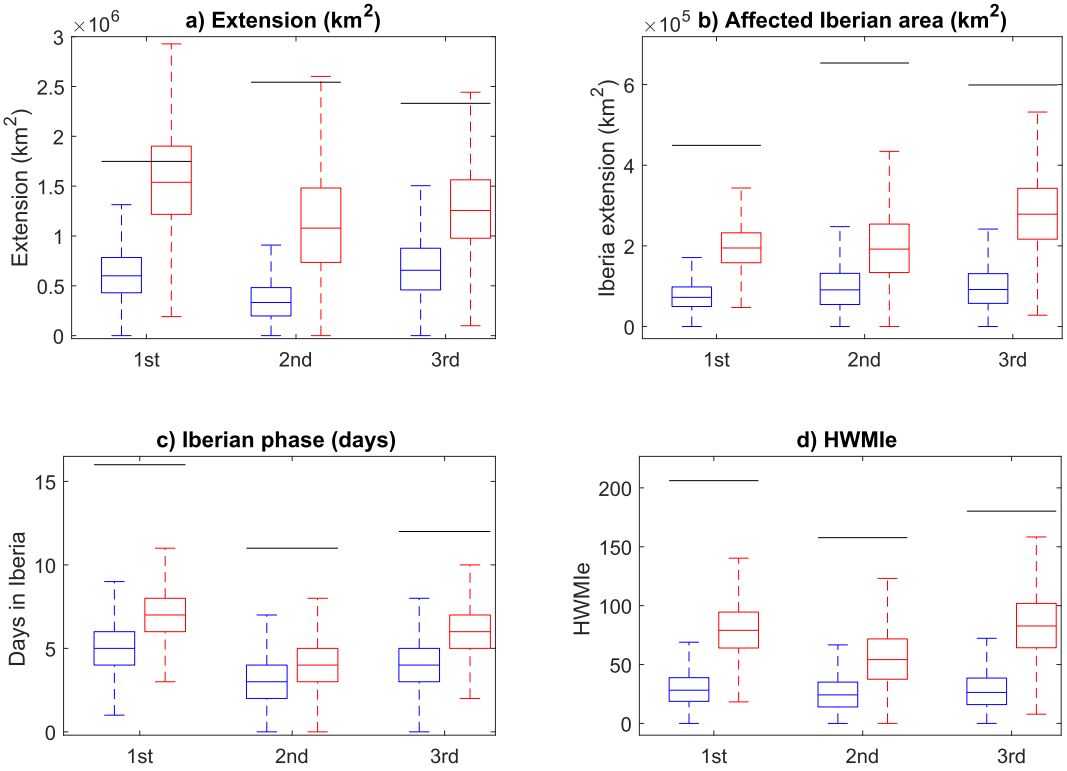

Fig. 9. Estimated distributions of: a) spatial extension of the HWE (in km^2); b) extension of the affected Iberian area (in km^2); c) Iberian phase (in days) and; d) HWMIe (dimensionless) for the top three Iberian HWEs, as derived from Z500 flow analogues of the past (1948–1978, blue boxplots) and present (1979–2017, red boxplots) subperiods. The boxplot represents the maximum/minimum value (top/bottom whisker), 75th, 50th and 25th percentile (top, middle, and bottom parts of the box). Black lines represent the observed parameter using the NCEP/NCAR reanalysis. (For interpretation of the references to colour in this figure legend, the reader is referred to the Web version of this article.)

4. Summary and conclusions

In this paper a new Lagragian-inspired heatwave (HW) detection algorithm was designed. It expands the HW analysis perspective allowing us to study the life-cycle of HWEs and the connection with synoptic weather patterns. Different to the classical Eulerian approaches, our method accounts for the spatial aggregation of local HW conditions (i.e. synoptic HW structures) and its temporal evolution (i.e. time-varying patterns). Similar to the approaches employed for the diagnosis of weather systems (storm tracks, blocks, etc.), this algorithm leads to an unambiguous and coherent identification of heatwave events (HWEs), which are characterized in terms of associated parameters (spatial extension, duration, intensity, trajectory, etc.). It is based on percentiles of the local temperature distribution only, with additional criteria for spatial extension, and temporal persistence and can be applied to any region and climate realm.

The algorithm is applied to ERA-Interim reanalysis data at 0.5°x0.5° resolution in order to obtain a catalogue and climatology of extended summer (June-September) Iberian HWEs for 1979–2017. Nevertheless, the results are qualitatively similar for other resolutions and reanalyses. The results indicate an averaged frequency of about five HWEs per year, leading to 16 summer days with HW conditions over Iberia (Iberian HWDs). These numbers are higher than those obtained in previous works with similar thresholds (Stefanon et al., 2012; Perkins, 2015; AEMET, 2018) due to the inclusion of September and the lack of a strict stationarity in the detection criteria of synoptic HWEs.

The analysis of the life-cycle of HWEs revealed that they are relatively long-lived, with a mean duration of 8.6 days. However, they only affected Iberia for 3.3 days on average, leading to short-lived HW conditions on local scales. Although Iberian HWEs are transient and spend most of their life-cycle elsewhere, more than half of them developed in Iberia, pointing it as a preferred region for HWE genesis.

When all Iberian HWEs are considered, there is large variability among events and preferred tracks do not clearly emerge. However, a clusterization of their mean temperature anomaly patterns yielded four groups with distinctive regional signatures and some characteristic HWE parameters. Overall, these clusters represent Atlantic, Subtropical, European and Mediterranean events that cause HW conditions over western, southern, northern and eastern Iberia, respectively. The Atlantic cluster includes the highest number of events of all groups, and highlights by a characteristic north-eastward path in the pre-Iberian phase. The Subtropical cluster tends to originate in northern Africa and embraces the lowest number of events, but with the largest extension. The European cluster mostly includes events that formed in Iberia, thus affecting the largest surface of the territory, and decayed rapidly while moving north-eastwards. HWEs belonging to the Mediterranean cluster are the most transient ones over Iberia, and show the lowest extension and intensity in this phase, but also the highest persistence in the post-Iberian phase, when they move eastwards, even growing in intensity and extension.

Iberian HWEs are associated with anomalous atmospheric circulation characterized mostly by a conspicuous positive Z500 anomaly aloft. The analysis of daily weather regimes (WRs) during Iberian HWDs revealed a clear predominance of WR4 (dominated by positive Z500 anomalies over western Europe), whose frequency of occurrence doubles as compared to climatology. Similar results are obtained for the regional groups of Iberian HWEs, indicating that the same WR can instigate HW conditions in different and relatively close areas depending on small changes in the synoptic configuration. However, as HWEs of each cluster display distinctive features and trajectories through their life-cycle, we report differences among the preferred WRs for the pre- and post-Iberian phases. WR1 is a characteristic precursor of Atlantic and Subtropical events, while WR2 and WR3 preferentially precede Mediterranean and European events, respectively. On seasonal scales,

regression models yielded significant relationships between the seasonal frequencies of WRs and regional Iberian HWDs, exception made for Subtropical events. The skill of WRs is relatively low (below 30% of explained variance) but could be improved by exploring other potential predictors of Iberian HWEs (e.g. soil moisture, sea surface temperatures, etc.). These results could be applied to seasonal forecasts of these predictors to infer the Iberian areas most affected by HWEs over the extended summer.

Using an event-oriented diagnostic (HWMIe) that integrates the spatial extent, intensity and persistence of HWEs, we also describe the top ten Iberian HWEs for the 1979–2017 period. These events are characterized by enhanced persistence and intensity, as compared to all Iberian HWEs. Half of them occurred in the 21st century, including well-known recent events such as 2003 and 2017. This apparent trend is supported by the long-term assessment of all Iberian HWEs, which reveals significant trends in the frequency of HWEs (+1.0 HWE decade^{-1}) and HWDs (+2.6 HWDs decade^{-1}) for 1979–2017. Nevertheless, we also found a slight tendency for Iberian HWEs to be more transient and affect smaller areas of Iberia, leading to decreases in the HWMIe index (none of these trends are significant, though). This unexpected result is explained by the significant increase of HWEs with parameters close to the imposed thresholds. Indeed, these characteristics are typical of Mediterranean events, whose increase explains most of the trends in Iberian HWEs, while contributing to lower current mean HWE parameters. In the absence of regional warming, these “edge-emerging” events would not have been detected as HWEs. This is supported by a flow analogue exercise of the three most outstanding HWEs, which unveils that recent warming has contributed to double some of their signatures (spatial extension, HWMIe), making these events more exceptional than they would have been in the past.

Acknowledgments

We acknowledge the European Centre for Medium-Range Weather Forecasts (ECMWF) for providing the ERA-Interim reanalysis data. NCEP/NCAR reanalysis data are provided by the Earth System Research Laboratory (ESRL) Physical Sciences Division, Boulder, Colorado (www.esrl.noaa.gov/psd). This work was supported by the Ministerio de Economía y Competitividad through the PALEOSTRAT (CGL2015-69699-R) project. A. Sánchez-Benítez was funded by grant FPU15/03958 from the Ministerio de Educación, Cultura y Deporte (MECD). The authors would like to thank J.M. Garrido-Pérez for his useful comments.

Appendix A. Supplementary data

Supplementary data to this article can be found online at https://doi.org/10.1016/j.wace.2019.100238.

References

Acero, F.J., García, J.A., Gallego, M.C., Parey, S., Dacunha-Castelle, D., 2014. Trends in summer extreme temperatures over the Iberian Peninsula using nonurban station data. J. Geophys. Res. Atmos 119, 39–53. https://doi.org/10.1002/2013JD020590.

AEMET, 2018. Olas de Calor en España desde 1975. Agencia Estatal de Meteorología. http://www.aemet.es/documentos/es/conocermas/recursos_en_linea/publicaciones_y_estudios/estudios/Olas_calor/Olas_Calor_ActualizacionOctubre2018.pdf. (Accessed 1 April 2019).

Álvarez-Castro, M.C., Faranda, D., Yiou, P., 2018. Atmospheric dynamics leading to west European summer hot temperatures since 1851. Complexity 2018, 1–10. https://doi.org/10.1155/2018/2494509.

Barriopedro, D., Fischer, E., Luterbacher, L., Trigo, R., García-Herrera, R., 2011. The hot summer of 2010: redrawing the temperature record map of Europe. Science 332 (6026), 220–224. https://doi.org/10.1126/science.1201224.

Byers, E., Gidden, M., Leclère, D., Balkovic, J., Burek, P., Ebi, K., Greve, P., Grey, D., Havlik, P., Hillers, A., Johnson, N., Kahil, T., Krey, V., Langan, S., Nakicenovic, N., Novak, R., Obersteiner, M., Pachauri, S., Palazzo, A., Parkinson, S., Rao, N.D., Rogelj, J., Satoh, Y., Wada, Y., Willaarts, B., Riahi, K., 2018. Global exposure and vulnerability to multi-sector development and climate change hotspots. Environ. Res. Lett. 13, 055012. https://doi.org/10.1088/1748-9326/aabf45.

Cassano, E.N., Lynch, A.H., Cassano, J.J., Koslow, M.R., 2006. Classification of synoptic patterns in the western Arctic associated with extreme events at Barrow, Alaska, USA. Clim. Res. 30, 83–97. https://doi.org/10.3354/cr030083.

Crane, R.G., Hewitson, B.C., 2003. Clustering and upscaling of station precipitation records to regional patterns using self-organizing maps (SOMs). Clim. Res. 25, 95–107. https://doi.org/10.3354/cr025095.

Dee, D., Uppala, S.M., Simmons, A.J., Berrisford, P., Poli, P., Kobayashi, S., Andrae, U., Balmaseda, M.A., Balsamo, G., Bauer, P., Bechtold, P., Beljaars, A.C.M., van de Berg, L., Bidlot, J., Bormann, N., Delsol, C., Dragani, R., Fuentes, M., Geer, A.J., Haimberger, L., Healy, S.B., Hersbach, H., Hólm, E.V., Isaksen, L.K., de Rosnay, P., Isaksen, L., Kållberg, P., Köhler, M., Matricardi, M., McNally, V., Monge-Sanz, B.M., Morcrette, J.-J., Park, B.-K., Peubey, C., de Rosnay, P., Tavolato, C., Thépaut, J.-N., Vitart, F., 2011. The ERA-Interim reanalysis: configuration and performance of the data assimilation system. Q. J. R. Meteorol. Soc. 137, 553–597. https://doi.org/10.1002/qj.828.

Fernández-Montes, S., Rodrigo, F.S., 2012. Trends in seasonal indices of daily temperature extremes in the Iberian Peninsula, 1929-2005. Int. J. Climatol. 32, 2320–2332. https://doi.org/10.1002/joc.3399.

Fernández-Montes, S., Rodrigo, F., 2015. Trends in surface air temperatures, precipitation and combined indices in the southeastern Iberian Peninsula (1970-2007). Clim. Res. 63, 43–60. https://doi.org/10.3354/cr01287.

Fouillet, A., Rey, G., Laurent, F., Pavillon, G., Bellec, S., Guilhenneue-Jouyaux, C., Clavel, J., Jougla, E., Hémon, D., 2006. Excess mortality related to the August 2003 heat wave in France. Int. Arch. Occup. Environ. Health. 80, 16–24. https://doi.org/10.1007/s00420-006-0089-4.

García-Herrera, R., Díaz, J., Trigo, R.M., Luterbacher, J., Fischer, E.M., 2010. A review of the european summer heat wave of 2003. Crit. Rev. Environ. Sci. Technol. 40, 267–306. https://doi.org/10.1080/10643380802238137.

García-Herrera, R., Barriopedro, D., 2018. Climate of the Mediterranean region. In: Oxford Research Encyclopedia of Climate Science. Oxford University Press USA. https://doi.org/10.1093/acrefore/9780190228620.013.509.

Gouveia, C.M., Bistinas, I., Liberato, M.L.R., Bastos, A., Koutsias, N., Trigo, R., 2016. The outstanding synergy between drought, heatwaves and fuel on the 2007 Southern Greece exceptional fire season. Agric. For. Meteorol 218–219, 135–145. https://doi.org/10.1016/j.agrformet.2015.11.023.

Hartmann, D.L., Klein Tank, A.M.G., Rusticucci, M., Alexander, L.V., Brönnimann, S., Charabi, Y., Dentener, F.J., Dlugokencky, E.J., Easterling, D.R., Kaplan, A., Soden, B.J., Thorne, P.W., Wild, M., Zhai, P.M., 2013. Observations: Atmosphere and Surface. Climate Change 2013: The Physical Science Basis. Contribution of Working Group I to the Fifth Assessment Report of the Intergovernmental Panel on Climate Change [Stocker, T.F., D. Qin, G.-K. Plattner, M. Tignor, S.K. Allen, J. Boschung, A. Nauels, Y. Xia, V. Bex and P.M. Midgley (eds.)]. Cambridge University Press, Cambridge, United Kingdom and New York, NY, USA.

Hodzic, A., Madronich, S., Bohn, B., Massie, S., Menut, L., Wiedinmyer, C., 2007. Wildfire particulate matter in Europe during summer 2003: Meso-scale modeling of smoke emissions, transport and radiative effects. Atmos. Chem. Phys. 7, 4043–4064. https://doi.org/10.5194/acp-7-4043-2007.

Hoegh-Guldberg, O., Jacob, D., Taylor, M., Bindi, M., Brown, S., Camilloni, I., Diedhiou, A., Djalante, R., Ebi, K.L., Engelbrecht, F., Guiot, J., Hijioka, Y., Mehrotra, S., Payne, A., Seneviratne, S.I., Thomas, A., Warren, R., Zhou, G., 2018. Impacts of 1.5 °C global warming on natural and human systems. In: Masson-Delmotte, V., Zhai, P., Pörtner, H.-O., Roberts, D., Skea, J., Shukla, P.R., Pirani, A., Moufouma-Okia, W., Péan, C., Pidcock, R., Connors, S., Matthews, J.B.R., Chen, Y., Zhou, X., Gomis, M.I., Lonnoy, E., Maycock, T., Tignor, M., Waterfield, T. (Eds.), Global Warming of 1.5 °C. An IPCC Special Report on the Impacts of Global Warming of 1.5 °C above Pre-industrial Levels and Related Global Greenhouse Gas Emission Pathways, in the Context of Strengthening the Global Response to the Threat of Climate Change, Sustainable Development, and Efforts to Eradicate Poverty. In Press.

Horton, D.E., Johnson, N.C., Singh, D., Swain, D.L., Rajaratnam, B., Diffenbaugh, N.S., 2015. Contribution of changes in atmospheric circulation patterns to extreme temperature trends. Nature 522, 465–469. https://doi.org/10.1038/nature14550.

Jézéquel, A., Cattiaux, J., Naveau, P., Radanovics, S., Ribes, A., Vautard, R., Vrac, M., Yiou, P., 2018a. Trends of atmospheric circulation during singular hot days in Europe. Environ. Res. Lett. 13 https://doi.org/10.1088/1748-9326/aab5da.

Jézéquel, A., Yiou, P., Radanovics, S., 2018b. Role of circulation in European heatwaves using flow analogues. Clim. Dyn. 50, 1145–1159. https://doi.org/10.1007/s00382-017-3667-0.

Kalnay, E., Kanamitsu, M., Kistler, R., Collins, W., Deaven, D., Gandin, L., Iredell, M., Saha, S., White, G., Woollen, J., Zhu, Y., Chelliah, M., Ebisuzaki, W., Higgins, W., Janowiak, J., Mo, K.C., Ropelewski, C., Wang, J., Leetmaa, A., Reynolds, R., Jenne, R., Joseph, D., 1996. The NCEP NCAR 40-year reanalysis project. Bull. Am. Meteorol. Soc. 77, 437–472. https://doi.org/10.1175/1520-0477(1996)077<0437:TNYRP>2.0.CO;2.

Kohonen, T., 2001. Self-Organizing Maps, third ed. Springer Verlag, New York.

Konovalov, I.B., Beekmann, M., Kuznetsova, I.N., Yurova, A., Zvyagintsev, A.M., 2011. Atmospheric impacts of the 2010 Russian wildfires: integrating modelling and measurements of an extreme air pollution episode in the Moscow region. Atmos. Chem. Phys. 11, 10031–10056. https://doi.org/10.5194/acp-11-10031-2011.

Lanzante, J.R., 1996. Resistant, robust and non-parametric techniques for the analysis of climate data: theory and examples, including applications to historical radiosonde station data. Int. J. Climatol. 16, 1197–1226. https://doi.org/10.1002/(SICI)1097-0088(199611)16:11<1197::AID-JOC89>3.0.CO;2-L.

Lelieveld, J., Proestos, Y., Hadjinicolaou, P., Tanarhte, M., Tyrlis, E., Zittis, G., 2016. Strongly increasing heat extremes in the Middle East and North Africa (MENA) in the

21st century. Clim. Change 137, 245–260. https://doi.org/10.1007/s10584-016-1665-6.
Lesk, C., Rowhani, P., Ramankutty, N., 2016. Influence of extreme weather disasters on global crop production. Nature 529, 84–87. https://doi.org/10.1038/nature16467.
Meehl, G., Tebaldi, C., 2004. More intense, more frequent, and longer lasting heat waves in the 21st century. Science 305, 994–997. https://doi.org/10.1126/science.1098704.
Morabito, M., Crisci, A., Messeri, A., Messeri, G., Betti, G., Orlandini, S., Raschi, A., Maracchi, G., 2017. Increasing heatwave hazards in the southeastern European union capitals. Atmosphere (Basel) 8 (115). https://doi.org/10.3390/atmos8070115.
Ordoñez, C., Barriopedro, D., García-Herrera, R., Sousa, P.M., Schnell, J., 2017. Regional responses of surface ozone in Europe to the location of high-latitude blocks and subtropical ridges. Atmos. Chem. Phys. 17, 3111–3131. https://doi.org/10.5194/acp-17-3111-2017.
Otto, F.E.L., Massey, N., Van Oldenborgh, G.J., Jones, R.G., Allen, M.R., 2012. Reconciling two approaches to attribution of the 2010 Russian heat wave. Geophys. Res. Lett. 39, 1–5. https://doi.org/10.1029/2011GL050422.
Peña-Ortiz, C., Barriopedro, D., García-Herrera, R., 2015. Multidecadal variability of the summer length in Europe. J. Clim. 28, 5375–5388. https://doi.org/10.1175/JCLI-D-14-00429.1.
Perkins, S.E., Alexander, L.V., 2013. On the measurement of heat waves. J. Clim. 26, 4500–4517. https://doi.org/10.1175/JCLI-D-12-00383.1.
Perkins, S.E., 2015. A review on the scientific understanding of heatwaves-Their measurement, driving mechanisms, and changes at the global scale. Atmos. Res. 164–165, 242–267. https://doi.org/10.1016/j.atmosres.2015.05.014.
Polade, S.D., Gershunov, A., Cayan, D.R., Dettinger, M.D., Pierce, D.W., 2017. Precipitation in a warming world: assessing projected hydro-climate changes in California and other Mediterranean climate regions. Sci. Rep. 7, 1–10. https://doi.org/10.1038/s41598-017-11285-y.
Ramos, A.M., Trigo, R.M., Santo, F.E., 2011. Evolution of extreme temperatures over Portugal: recent changes and future scenarios. Clim. Res. 48, 177–192. https://doi.org/10.3354/cr00934.
Rodríguez-Puebla, C., Encinas, A.H., García-Casado, L.A., Nieto, S., 2010. Trends in warm days and cold nights over the Iberian Peninsula: relationships to large-scale variables. Clim. Change 100, 667–684. https://doi.org/10.1007/s10584-009-9721-0.
Russo, S., Sillmann, J., Fischer, E.M., 2015. Top ten European heatwaves since 1950 and their occurrence in the coming decades. Environ. Res. Lett. 10, 124003. https://doi.org/10.1088/1748-9326/10/12/124003.
Sánchez-Benítez, A., García-Herrera, R., Barriopedro, D., Sousa, P.M., Trigo, R.M., 2018. June 2017: The Earliest European Summer Mega-heatwave of Reanalysis Period. Geophys. Res. Lett. 45 https://doi.org/10.1002/2018GL077253.
Shepherd, T.G., 2016. A common framework for approaches to extreme event attribution. Curr. Clim. Chang. Reports 2, 28–38. https://doi.org/10.1007/s40641-016-0033-y.
Sousa, P.M., Trigo, R.M., Barriopedro, D., Soares, P.M.M., Santos, J.A., 2018. European temperature responses to blocking and ridge regional patterns. Clim. Dyn. 50, 457–477. https://doi.org/10.1007/s00382-017-3620-2.
Sousa, P.M., Barriopedro, D., Ramos, A.M., García-Herrera, R., Espírito-Santo, F., Trigo, R.M., 2019. Saharan air intrusions as a relevant mechanism for Iberian heatwaves: the record breaking events of August 2018 and 147 June 2019. Weather and Climate Extremes (Accepted).
Stefanon, M., D'Andrea, F., Drobinski, P., 2012. Heatwave classification over Europe and the Mediterranean region. Environ. Res. Lett. 7 https://doi.org/10.1088/1748-9326/7/1/014023.
Stott, P.A., Allen, M.R., Jones, G.S., 2003. Estimating signal amplitudes in optimal fingerprinting. Part II: application to general circulation models. Clim. Dyn. 21, 493–500. https://doi.org/10.1007/s00382-003-0314-8.
Stott, P.A., Christidis, N., Otto, F.E.L., Sun, Y., Vanderlinden, J.P., van Oldenborgh, G.J., Vautard, R., von Storch, H., Walton, P., Yiou, P., Zwiers, F.W., 2016. Attribution of extreme weather and climate-related events. Wiley Interdiscip. Rev. Clim. Chang 7, 23–41. https://doi.org/10.1002/wcc.380.
Tomczyk, A.M., Półrolniczak, M., Bednorz, E., 2017. Circulation conditions' effect on the occurrence of heatwaves in Western and Southwestern Europe. Atmosphere (Basel) 8. https://doi.org/10.3390/atmos8020031.
Tressol, M., Ordonez, C., Zbinden, R., Brioude, J., Thouret, V., Mari, C., Nedelec, P., Cammas, J.P., Smit, H., Patz, H.W., Volz-Thomas, A., 2008. Air pollution during the 2003 European heat wave as seen by MOZAIC airliners. Atmos. Chem. Phys. 8, 2133–2150. https://doi.org/10.5194/acp-8-2133-2008.
Vautard, R., Honoré, C., Beekmann, M., Rouil, L., 2005. Simulation of ozone during the August 2003 heat wave and emission control scenarios. Atmos. Environ. 39, 2957–2967. https://doi.org/10.1016/j.atmosenv.2005.01.039.
Vautard, R., Yiou, P., Otto, F., Stott, P., Christidis, N., van Oldenborgh, G.J., Schaller, N., 2016. Attribution of human-induced dynamical and thermodynamical contributions in extreme weather events. Environ. Res. Lett. 11, 114009. https://doi.org/10.1088/1748-9326/11/11/114009.
Wilks, D., 2011. Statistical Methods in the Atmospheric Sciences, third ed. Academic Press, New York.
Yiou, P., Jézéquel, A., Naveau, P., Otto, F.E.L., Vautard, R., Vrac, M., 2017. A statistical framework for conditional extreme event attribution. Adv. Stat. Climatol. Meteorol. Oceanogr 3, 17–31. https://doi.org/10.5194/ascmo-3-17-2017.
Zschenderlein, P., Fragkoulidis, G., Fink, A.H., Wirth, V., 2018. Large-scale Rossby wave and synoptic-scale dynamic analyses of the unusually late 2016 heatwave over Europe. Weather 73, 275–283. https://doi.org/10.1002/wea.3278.